





Article

Noninvasive Assessment of Neuromechanical Coupling and Mechanical Efficiency of Parasternal Intercostal Muscle during Inspiratory Threshold Loading

Manuel Lozano-García ^{1,2,3,*}, Luis Estrada-Petrocelli ^{1,2,4}, Abel Torres ^{1,2,3}, Gerrard F. Rafferty ⁵, John Moxham ⁵, Caroline J. Jolley ^{5,6,†} and Raimon Jané ^{1,2,3,†}

- ¹ Institute for Bioengineering of Catalonia (IBEC), The Barcelona Institute of Science and Technology (BIST), UPC Campus Diagonal-Besòs, Av. d'Eduard Maristany 10–14, 08019 Barcelona, Spain; lestrada@ibecbarcelona.eu (L.E.-P.); atorres@ibecbarcelona.eu (A.T.); rjane@ibecbarcelona.eu (R.J.)
 - ² Biomedical Research Networking Centre in Bioengineering, Biomaterials and Nanomedicine (CIBER-BBN), 08028 Barcelona, Spain
 - ³ Department of Automatic Control (ESAI), Universitat Politècnica de Catalunya (UPC)-Barcelona Tech, 08028 Barcelona, Spain
 - ⁴ Facultad de Ingeniería, Universidad Latina de Panamá, Panama City 0823-00923, Panama
 - ⁵ Centre for Human & Applied Physiological Sciences, School of Basic & Medical Biosciences, Faculty of Life Sciences & Medicine, King's College London, King's Health Partners, London SE1 9RT, UK; gerrard.rafferty@kcl.ac.uk (G.F.R.); john.moxham@kcl.ac.uk (J.M.); caroline.jolley@kcl.ac.uk (C.J.J.)
 - ⁶ King's College Hospital NHS Foundation Trust, King's Health Partners, London SE5 9RS, UK
- * Correspondence: mlozano@ibecbarcelona.eu; Tel.: +34-695-119-250
† C.J.J. and R.J. contributed equally to this work.



Citation: Lozano-García, M.; Estrada-Petrocelli, L.; Torres, A.; Rafferty, G.F.; Moxham, J.; Jolley, C.J.; Jané, R. Noninvasive Assessment of Neuromechanical Coupling and Mechanical Efficiency of Parasternal Intercostal Muscle during Inspiratory Threshold Loading. *Sensors* **2021**, *21*, 1781. <https://doi.org/10.3390/s21051781>

Academic Editor: Marco Di Rienzo

Received: 11 January 2021

Accepted: 28 February 2021

Published: 4 March 2021

Publisher's Note: MDPI stays neutral with regard to jurisdictional claims in published maps and institutional affiliations.



Copyright: © 2021 by the authors. Licensee MDPI, Basel, Switzerland. This article is an open access article distributed under the terms and conditions of the Creative Commons Attribution (CC BY) license (<https://creativecommons.org/licenses/by/4.0/>).

Abstract: This study aims to investigate noninvasive indices of neuromechanical coupling (NMC) and mechanical efficiency (MEff) of parasternal intercostal muscles. Gold standard assessment of diaphragm NMC requires using invasive techniques, limiting the utility of this procedure. Noninvasive NMC indices of parasternal intercostal muscles can be calculated using surface mechanomyography (sMMG_{para}) and electromyography (sEMG_{para}). However, the use of sMMG_{para} as an inspiratory muscle mechanical output measure, and the relationships between sMMG_{para}, sEMG_{para}, and simultaneous invasive and noninvasive pressure measurements have not previously been evaluated. sEMG_{para}, sMMG_{para}, and both invasive and noninvasive measurements of pressures were recorded in twelve healthy subjects during an inspiratory loading protocol. The ratios of sMMG_{para} to sEMG_{para}, which provided muscle-specific noninvasive NMC indices of parasternal intercostal muscles, showed nonsignificant changes with increasing load, since the relationships between sMMG_{para} and sEMG_{para} were linear ($R^2 = 0.85$ (0.75–0.9)). The ratios of mouth pressure (P_{mo}) to sEMG_{para} and sMMG_{para} were also proposed as noninvasive indices of parasternal intercostal muscle NMC and MEff, respectively. These indices, similar to the analogous indices calculated using invasive transdiaphragmatic and esophageal pressures, showed nonsignificant changes during threshold loading, since the relationships between P_{mo} and both sEMG_{para} ($R^2 = 0.84$ (0.77–0.93)) and sMMG_{para} ($R^2 = 0.89$ (0.85–0.91)) were linear. The proposed noninvasive NMC and MEff indices of parasternal intercostal muscles may be of potential clinical value, particularly for the regular assessment of patients with disordered respiratory mechanics using noninvasive wearable and wireless devices.

Keywords: inspiratory threshold loading; neuromechanical coupling; parasternal intercostal muscles; respiratory pressure; surface electromyography; surface mechanomyography

1. Introduction

Evaluating respiratory muscle function contributes to enhancing the diagnosis, phenotyping, and monitoring of patients with respiratory symptoms and neuromuscular diseases [1]. Inspiratory pressure generation is dependent on the level of muscle electrical

activation and the transduction of this electrical activation into pressure, termed neuromechanical coupling (NMC). Poor transduction of inspiratory muscle electrical activation into pressure, neuromechanical uncoupling, is common in obstructive lung disease [2–4], and has been related to the perception of dyspnea in both obstructive lung disease [5] and in neuromuscular disease [6]. Measuring inspiratory muscle NMC is therefore clinically important for the assessment of patients with disordered respiratory mechanics.

Inspiratory muscle NMC estimation requires simultaneous measurement of muscle electrical activation and mechanical output. To date, most studies reporting inspiratory muscle NMC have focused on the diaphragm, the principal inspiratory muscle [7]. The gold standard measurement of diaphragm electrical activation and mechanical output involves the use of invasive techniques, including crural diaphragm electromyography using a multipair esophageal electrode catheter (oesEMG_{di}) to assess neural respiratory drive [8], and the balloon-catheter technique to measure transdiaphragmatic pressure (P_{di}) [1]. However, the utility of these techniques is limited by the invasive nature of the measurements, subject tolerance, and requirement for specialist equipment and training. In this regard, noninvasive measurement of inspiratory muscle NMC would facilitate the assessment of respiratory muscle function.

Parasternal intercostal muscles are obligatory muscles of inspiration and their activation is coupled to that of the diaphragm [9]. Measurements of surface electromyography of the parasternal intercostal muscles (sEMG_{para}) have been shown to provide a robust measure of load on the respiratory muscle pump and to strongly correlate with measurements of oesEMG_{di} [10–12]. Measurements of sEMG_{para} have also been related to breathlessness in both healthy subjects [3,12] and patients with respiratory disease [3,12–15]. Therefore, and given the advantage of being noninvasive, sEMG_{para} has been proposed as an alternative measure for the assessment of neural respiratory drive [10,11].

Surface mechanomyography (sMMG) measures muscle surface vibrations due to motor unit mechanical activity [16], and represents the mechanical counterpart of motor unit electrical activity, as measured by surface electromyography (sEMG). In non-respiratory skeletal muscles, the ratio of sMMG to sEMG has been proposed for the assessment of muscle electromechanical efficiency [17,18]. In the respiratory system, sMMG and pressure represent different mechanical states of inspiratory muscles, the latter being a more global measure of respiratory muscle mechanical output. We have recently used sMMG and sEMG measurements from lower chest wall intercostal spaces (sMMG_{lic} and sEMG_{lic}, respectively) to provide noninvasive indices of lower chest wall inspiratory muscle NMC [19], which did not change significantly with increasing inspiratory load due to the linear relationship between sMMG_{lic} and sEMG_{lic} measurements. Measurements of sMMG_{lic} have also been used, in combination with measurements of mouth pressure (P_{mo}), to calculate the mechanical efficiency (MEff) of lower chest wall inspiratory muscles, that is the transformation of muscle mechanical activation into pressure generation, in healthy subjects and patients with chronic obstructive pulmonary disease (COPD) [20]. Lower chest wall recordings are, however, less easily accessible and more contaminated by non-respiratory chest wall and abdominal muscle activation than parasternal intercostal recordings [21,22]. Nevertheless, the use of parasternal intercostal muscle sMMG (sMMG_{para}) as a noninvasive measure of inspiratory muscle mechanical output has not previously been investigated.

Inspiratory muscle mechanical output is usually estimated as pressure. Gold standard P_{di} measurements are derived from simultaneous measurements of gastric (P_{gas}) and esophageal (P_{oes}) pressures ($P_{di} = P_{gas} - P_{oes}$). Since P_{di} is specific to the diaphragm, P_{di} has been widely used, together with oesEMG_{di}, for the assessment of diaphragm NMC [4,12,19,23–26]. Measurements of P_{oes} alone are, however, not specific to the diaphragm and are influenced by the activation of all inspiratory muscles [1]. Compared to P_{di} , P_{oes} is therefore expected to better reflect the mechanical output of extra-diaphragmatic muscles, including the parasternal intercostal muscles. Moreover, P_{mo} , which provides a noninvasive approximation of P_{oes} [1], could be used to obtain noninvasive indices of NMC and MEff of parasternal intercostal muscles. However, to our knowledge, no study

has evaluated the relationships among simultaneous invasive and noninvasive measurements of respiratory pressures and both sEMG_{para} and sMMG_{para} measurements for the assessment of NMC and MEff of parasternal intercostal muscles.

The principal aim of this study was therefore to investigate the use of sMMG_{para} as a novel noninvasive index of parasternal intercostal muscle mechanical output. In addition, we wished to examine the relationship between sMMG_{para} and sEMG_{para} to provide muscle-specific noninvasive indices of NMC of parasternal intercostal muscles, in healthy subjects during an incremental inspiratory threshold loading protocol. We hypothesized that, as in lower chest wall inspiratory muscles, there would be a linear relationship between measurements of sMMG_{para} and sEMG_{para} in healthy subjects, thus resulting in nonsignificant changes in NMC of parasternal intercostal muscles (the ratio of sMMG_{para} to sEMG_{para} measurements) during threshold loading. We also aimed to explore the relationship between measurements of sEMG_{para} and sMMG_{para} and both invasive and noninvasive measurements of respiratory pressures, to obtain indices of NMC and MEff of parasternal intercostal muscles.

2. Materials and Methods

2.1. Data Acquisition and Preprocessing

2.1.1. Measurements

This study was carried out in the Respiratory Physiology Laboratory at the King's College London, King's College Hospital, London, United Kingdom. Ethics approval was obtained from the National Health Service Health Research Authority (National Research Ethics Service Committee London—Dulwich 05/Q0703) and the study was conducted in accordance with the Declaration of Helsinki.

All recordings were obtained from 12 healthy subjects, including 6 male and 6 female, with no medical history of neuromuscular or cardiorespiratory disease and with the following characteristics (median (interquartile range)): age 33 (30–39) years, body mass index (BMI) 22.2 (20.6–24.2) kg/m², forced expiratory volume in 1 second 98% (95–106%) % of predicted, and forced expiratory volume in 1 second/forced vital capacity 82% (74–84%) % of predicted [19]. Written consent was provided by all subjects prior to study participation.

sEMG_{para} was acquired using a pair of surface electrodes in bipolar configuration located bilaterally in the second intercostal space [10,27]. The sEMG_{para} recordings were amplified, high-pass filtered with a cut-off frequency of 10 Hz, and alternating current coupled. sMMG_{para} was acquired using a triaxial accelerometer (TSD109C2; BIOPAC Systems Inc, Goleta, CA, USA) attached to the skin in the second intercostal space, between the sEMG_{para} electrodes and close to the right one. P_{gas} and P_{oes} were acquired using a catheter tip pressure transducer (CTO-2; Gaeltec Devices Ltd., Dunvegan, UK), as previously described [12]. Airflow was acquired using a pneumotachometer (4830; Hans Rudolph Inc, Shawnee, KS, USA). P_{mo} was acquired using a differential pressure transducer (MP45; Validyne Engineering, Northridge, CA, USA) connected to a side port of the pneumotachometer.

All respiratory signals were acquired using a 16-bit analog-to-digital converter (PowerLab 16/35; ADInstruments Ltd, Oxford, UK) at a sampling frequency of 4000 Hz (sEMG_{para}), 2000 Hz (sMMG_{para}), and 100 Hz (pressures and airflow). LabChart software (Version 7.2, ADInstruments Pty, Colorado Springs, CO, USA) was used to manage the signal acquisition.

2.1.2. Acquisition Protocol

Initially, each participant carried out two types of maximal volitional respiratory maneuvers: maximal static inspiratory pressure (P_{Imax}) [1] and maximal inspirations to total lung capacity [10,28]. These maneuvers were performed several times to ensure each subject's maximal volitional effort. All signals were recorded during two minutes of resting breathing (L0). After that, each participant carried out an inspiratory threshold loading protocol at inspiratory threshold loads ranging from 12% (L1) to 60% (L5) of P_{Imax}, in

increments of 12%, as we previously described [19]. Inspiratory loads were generated using an electronic inspiratory muscle trainer (POWERbreathe K5; POWERbreathe International Ltd, Southam, UK) attached to the distal end of the pneumotachometer. Subjects breathed through the pneumotachometer and performed 30 breaths against each inspiratory load, with a resting period in between to allow all measurements to return to baseline.

2.1.3. Data Preprocessing

All data were processed and analyzed in MATLAB (The MathWorks, Inc., vR2020a, Natick, MA, USA). sEMG_{para} signals were down-sampled at 2000 Hz and filtered between 10 and 600 Hz. Removal of 50 Hz interference was performed by means of a comb filter. sMMG_{para} signals were down-sampled at 500 Hz and filtered between 5 and 40 Hz. The three acceleration components recorded by the accelerometer were root sum squared to calculate the magnitude of the sMMG_{para} signal ($|sMMG_{para}|$).

A zero-crossing threshold-based detector was applied to P_{mo} in order to detect inspiratory and expiratory segments during resting breathing and each threshold load for subsequent inspiratory muscle activity estimation. For each respiratory cycle, the following parameters were calculated: inspiratory time, inspiratory time/total respiratory cycle time, inspiratory volume (i.e., the area under the curve of the inspiratory flow), and breathing frequency. The median values of all respiratory cycles were then calculated separately for L0–L5, and 10 respiratory cycles that contained the four parameters nearest to the median values were automatically selected, resulting in 60 respiratory cycles per subject.

The moving minimum of the P_{di} signal and the moving maximum of the P_{oes} signal were calculated using a moving window of 1.5 times the maximum inspiratory time of each load, and subtracted from the P_{di} and P_{oes} signals, respectively.

2.2. Data Processing

2.2.1. Inspiratory Muscle Activity Estimation

Inspiratory muscle activity estimation has usually been based on conventional amplitude estimators, such as the average rectified value (ARV) or the root mean square (RMS) [28,29]. However, when applied to myographic respiratory signals, these parameters are greatly affected by cardiac activity, and therefore prior rejection of signal segments that contain cardiac noise is required. Fixed sample entropy (fSampEn) has been demonstrated to reduce cardiac activity in myographic respiratory signals [30,31], allowing inspiratory muscle activity to be estimated without the need for prior rejection of cardiac artefacts. fSampEn consists in calculating sample entropy within a moving window over a signal, using a fixed tolerance value for all windows [30]. In this way, fSampEn is sensitive to variations in both signal complexity and signal amplitude. Therefore, like ARV and RMS, fSampEn can track amplitude variations in myographic respiratory signals. Furthermore, since cardiac artifacts exhibit a more deterministic pattern compared to respiratory EMG and MMG signals, fSampEn also inherently reduces cardiac activity, and therefore it is less influenced by cardiac artefacts than ARV or RMS.

In this study, fSampEn was calculated for the sEMG_{para} (fSEsEMG_{para}) and $|sMMG_{para}|$ (fSE $|sMMG_{para}|$) signals, using the optimal fSampEn parameters that we previously described for respiratory muscle activity estimation (i.e., a moving window of 500 ms with a 50 ms step, m equal to 2, and r equal to 0.3 (sEMG_{para}) and 0.5 ($|sMMG_{para}|$) times the global standard deviation of each signal) [32]. Inspiratory muscle activity was then estimated for each respiratory cycle as the mean inspiratory P_{di} , P_{oes} , P_{mo} , fSE $|sMMG_{para}|$, and fSEsEMG_{para}. The mean values of fSE $|sMMG_{para}|$ and fSEsEMG_{para} were expressed as percentages of their respective largest mean values obtained during the inspiratory threshold loading protocol and the two maximal volitional maneuvers (fSE $|sMMG_{para}|$ %_{max} and fSEsEMG_{para} %_{max}).

2.2.2. Neuromechanical Coupling and Mechanical Efficiency

NMCs of parasternal intercostal muscles were calculated as the ratios of $fSE | sMMG_{para} | \%_{max}$, mean P_{di} , mean P_{oes} , and mean P_{mo} to $fSEsEMG_{para}\%_{max}$ ($NMC_{MMG-EMG_{para}}$, $NMC_{P_{di}-EMG_{para}}$, $NMC_{P_{oes}-EMG_{para}}$, and $NMC_{P_{mo}-EMG_{para}}$, respectively). MEffs of parasternal intercostal muscles were calculated as the ratios of mean P_{di} , mean P_{oes} , and mean P_{mo} to $fSE | sMMG_{para} | \%_{max}$ ($MEff_{P_{di}-MMG_{para}}$, $MEff_{P_{oes}-MMG_{para}}$, and $MEff_{P_{mo}-MMG_{para}}$, respectively). The average value of the ten respiratory cycles selected for resting breathing and each load was calculated for all NMCs and MEffs.

2.3. Statistical Analysis

All data correspond to median and interquartile range. Changes in respiratory pressures, $fSE | sMMG_{para} | \%_{max}$, and $fSEsEMG_{para}\%_{max}$ with increasing threshold load were assessed using Friedman tests followed by multiple Wilcoxon signed-rank tests with Bonferroni adjusted p -values.

An increasing NMC with increasing load can be well explained by an exponential relationship between the measurements involved [19]. By contrast, a NMC that remains almost constant or increases slightly with increasing load indicates that the relationship between the measurements involved can be well explained by a linear model. Therefore, in this study, the relationships between measurements of respiratory pressures, $fSE | sMMG_{para} | \%_{max}$, and $fSEsEMG_{para}\%_{max}$ were assessed individually using both linear and exponential regression models, together with Spearman's rank correlation coefficients (ρ). Moreover, changes in NMCs and MEffs during threshold loads L1–L5 were assessed using Friedman tests, followed by multiple Wilcoxon signed-rank tests with Bonferroni adjustment for multiple comparisons, with the same method that we previously described [19]. The significance level for all statistical tests was set at 0.05.

3. Results

Figure 1 shows an example of respiratory signals recorded in a healthy subject during resting breathing and the inspiratory threshold loading protocol.

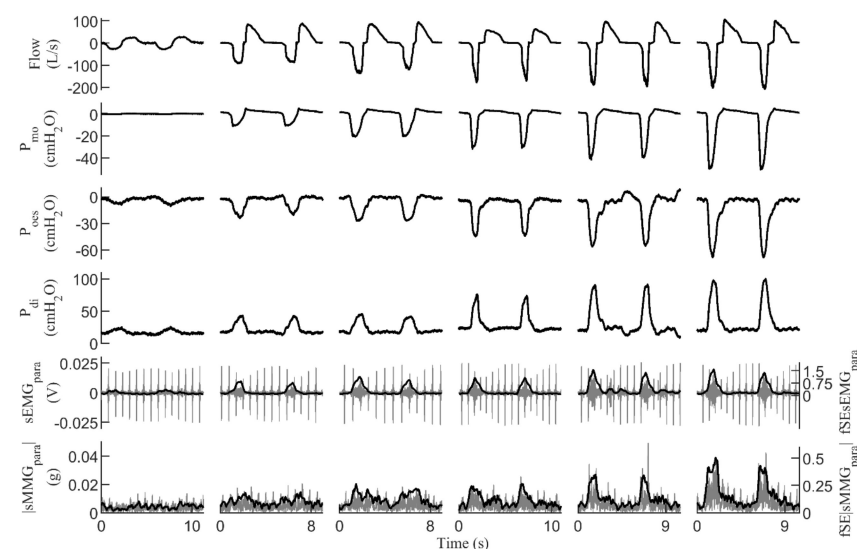


Figure 1. Signals recorded during the inspiratory threshold loading protocol in a healthy subject. Two respiratory cycles are shown for quiet resting breathing and inspiratory threshold loads at 12%, 24%, 36%, 48%, and 60% of maximal static inspiratory pressure. For the $sEMG_{para}$ and $|sMMG_{para}|$ signals, the corresponding fixed sample entropy time-series ($fSEsEMG_{para}$ and $fSE | sMMG_{para} |$ respectively) are also shown. P_{mo} = mouth pressure, P_{oes} = esophageal pressure, P_{di} = transdiaphragmatic pressure, $sEMG_{para}$ = surface electromyography of the parasternal intercostal muscles, $|sMMG_{para}|$ = surface mechanomyography of the parasternal intercostal muscles.

3.1. Respiratory Pressures

Median (interquartile range (IQR)) P_Imax for the group was 87.0 (78.0–116.5) cmH₂O. The inspiratory threshold loads increased from 10.5 (9.5–14.0) cmH₂O during load L1 to 52.0 (47.0–70.0) cmH₂O during load L5. Mean P_{di}, mean P_{oes}, and mean P_{mo} increased significantly between successive loads during the inspiratory threshold loading protocol (Figure 2). Although all pressures increased in parallel during threshold loading, mean P_{mo} was consistently lower than mean P_{oes} and mean P_{di}.

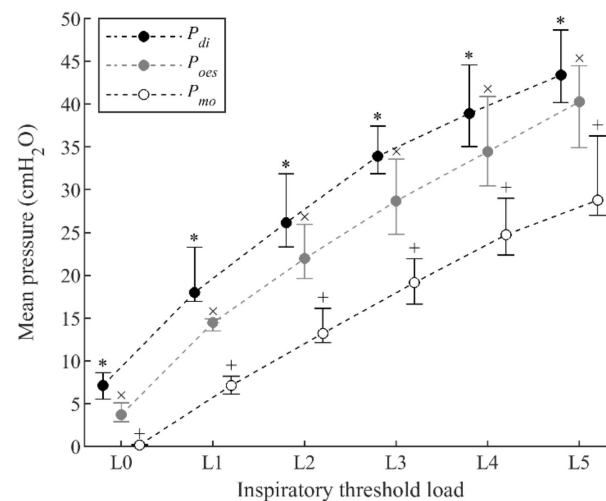


Figure 2. Evolution of respiratory pressures during progressive inspiratory threshold loading. Data points represent median and interquartile (IQR) range of the 12 subjects for each load. All data points with the same symbol (*, ×, or +) were significantly different to each other.

3.2. sMMG and sEMG of Parasternal Intercostal Muscles during Threshold Loading

Measurements of fSE | sMMG_{para} | %_{max} increased progressively from 10.9% (9.4–14.8%) during resting breathing to 64.7% (54.2–75.9%) during load L5 (Figure 3). Similarly, measurements of fSEsEMG_{para}%_{max} increased from 13.5% (10.4–17.6%) during resting breathing to 72.2% (67.2–80.9%) during load L5. Increases in fSE | sMMG_{para} | %_{max} and fSEsEMG_{para}%_{max} were statistically significant between successive loads, except between loads L3 and L4 in fSEsEMG_{para}%_{max}, and between loads L4 and L5 in both fSE | sMMG_{para} | %_{max} and fSEsEMG_{para}%_{max} measurements. Moreover, although fSE | sMMG_{para} | %_{max} and fSEsEMG_{para}%_{max} increased in parallel during threshold loading, fSE | sMMG_{para} | %_{max} was consistently lower than fSEsEMG_{para}%_{max}.

3.3. Noninvasive Measurements of Neuromechanical Coupling and Mechanical Efficiency of Parasternal Intercostal Muscles

Having an increasing or almost constant pattern of NMC and MEff indices with increasing load depends on whether the relationship between the measurements involved is exponential or linear respectively, as we previously described [19]. Accordingly, the relationships between measurements of respiratory pressures, fSE | sMMG_{para} | %_{max}, and fSEsEMG_{para}%_{max} were firstly assessed individually using both linear and exponential regression models. Secondly, the evolution of the group NMC and MEff indices during threshold loads L1–L5 was assessed using Friedman tests, followed by multiple Wilcoxon signed-rank tests with Bonferroni adjustment for multiple comparisons.

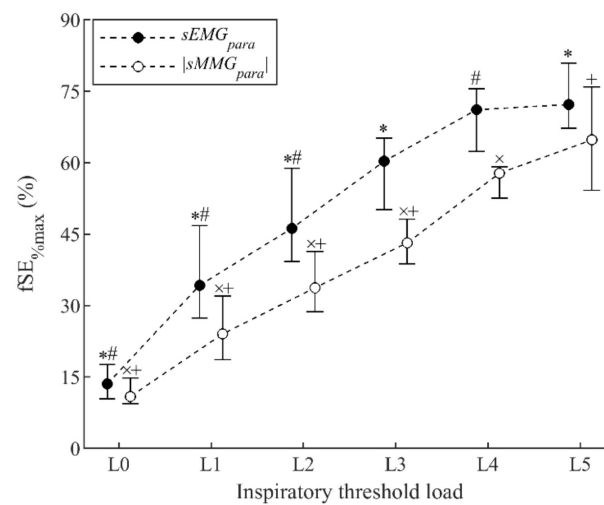


Figure 3. Fixed sample entropy measurements of surface mechanomyography ($fSE_{|sMMG_{para}| \%max}$) and surface electromyography ($fSE_{sEMG_{para} \%max}$) of the parasternal intercostal muscles during inspiratory threshold loading. Data points represent median and interquartile range of the 12 subjects for each load. All data points with the same symbol (*, #, ×, or +) were significantly different to each other.

The relationship between $fSE_{|sMMG_{para}| \%max}$ and $fSE_{sEMG_{para} \%max}$ measurements shown in Figure 4a was firstly assessed. Very strong positive correlations between $fSE_{|sMMG_{para}| \%max}$ and $fSE_{sEMG_{para} \%max}$ were found individually (Table 1). Individual linear and exponential regression results shown in Table 2 indicate that the linear model, besides being simpler, performed slightly better than the exponential model to describe the relationships between $fSE_{|sMMG_{para}| \%max}$ and $fSE_{sEMG_{para} \%max}$. The evolution of the group $NMC_{MMG-EMG_{para}}$ during progressive inspiratory threshold loading is shown in Figure 4b. Slight and nonsignificant increases were found in $NMC_{MMG-EMG_{para}}$ between loads L1 and L5, confirming that the relationship between $fSE_{|sMMG_{para}| \%max}$ and $fSE_{sEMG_{para} \%max}$ can be well explained by a linear model.

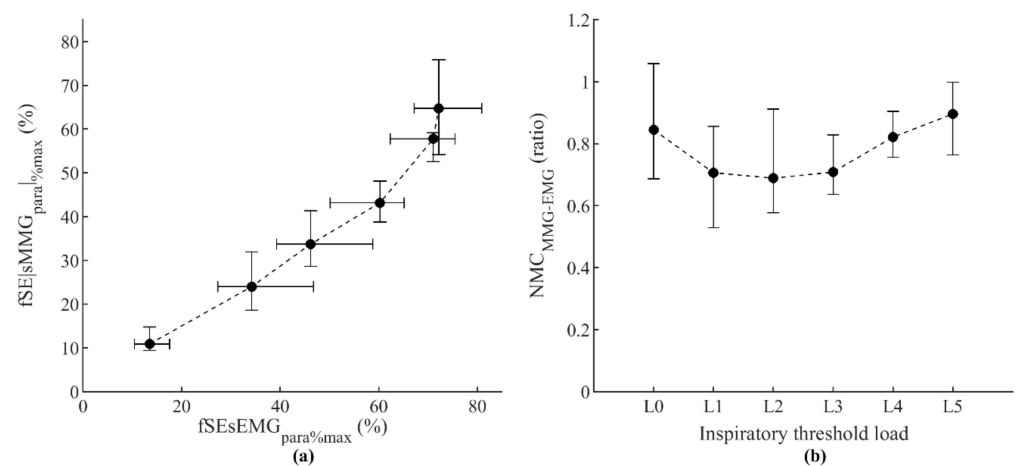


Figure 4. Relationship between fixed sample entropy measurements of surface mechanomyography ($fSE_{|sMMG_{para}| \%max}$) and surface electromyography ($fSE_{sEMG_{para} \%max}$) of the parasternal intercostal muscles (a) and the corresponding neuromechanical coupling ratio ($NMC_{MMG-EMG_{para}}$) (b), during the incremental inspiratory threshold loading protocol. Data points represent median and interquartile range of the 12 subjects for each load.

Table 1. Spearman's ρ between measurements of respiratory pressures, $fSE | sMMG_{para} | \%max$, and $fSEsEMG_{para \%max}$.

ID	$fSEsEMG_{para \%max}$	$fSEsEMG_{para \%max}$	$fSEsEMG_{para \%max}$	$fSEsEMG_{para \%max}$	$fSE sMMG_{para} \%max$	$fSE sMMG_{para} \%max$	$fSE sMMG_{para} \%max$
	$fSE sMMG_{para} \%max$	Mean P_{di}	Mean P_{oes}	Mean P_{mo}	Mean P_{di}	Mean P_{oes}	Mean P_{mo}
1	0.88	0.90	0.89	0.89	0.89	0.90	0.92
2	0.93	0.94	0.97	0.95	0.89	0.93	0.93
3	0.95	0.87	0.95	0.97	0.82	0.92	0.95
4	0.95	0.92	0.95	0.92	0.94	0.96	0.95
5	0.96	0.96	0.94	0.94	0.96	0.96	0.95
6	0.93	0.88	0.89	0.87	0.92	0.93	0.92
7	0.98	0.98	0.96	0.96	0.97	0.97	0.97
8	0.97	0.98	0.98	0.98	0.96	0.96	0.97
9	0.88	0.91	0.91	0.92	0.92	0.91	0.91
10	0.91	0.82	0.85	0.84	0.91	0.94	0.94
11	0.80	0.76	0.77	0.74	0.96	0.97	0.96
12	0.87	0.91	0.90	0.88	0.91	0.92	0.92
Median (IQR)	0.93 (0.88–0.96)	0.91 (0.88–0.95)	0.92 (0.89–0.96)	0.92 (0.87–0.96)	0.92 (0.90–0.96)	0.94 (0.92–0.96)	0.94 (0.92–0.95)

IQR = interquartile range, P_{di} = transdiaphragmatic pressure, P_{oes} = esophageal pressure, P_{mo} = mouth pressure, $fSEsEMG_{para \%max}$ = fixed sample entropy measurements of surface electromyography of the parasternal intercostal muscles, $fSE | sMMG_{para} | \%max$ = fixed sample entropy measurements of surface mechanomyography of the parasternal intercostal muscles. All correlations were statistically significant.

Table 2. Adjusted R^2 of the linear and exponential regression models to describe the relationships between measurements of respiratory pressures, $fSE | sMMG_{para} | \%max$, and $fSEsEMG_{para \%max}$.

ID	$fSEsEMG_{para \%max}$		$fSEsEMG_{para \%max}$		$fSEsEMG_{para \%max}$		$fSEsEMG_{para \%max}$		$fSE sMMG_{para} \%max$		$fSE sMMG_{para} \%max$		$fSE sMMG_{para} \%max$	
	$fSE sMMG_{para} \%max$		Mean P_{di}		Mean P_{oes}		Mean P_{mo}		Mean P_{di}		Mean P_{oes}		Mean P_{mo}	
	Lin.	Exp.	Lin.	Exp.	Lin.	Exp.	Lin.	Exp.	Lin.	Exp.	Lin.	Exp.	Lin.	Exp.
1	0.74	0.69	0.81	0.78	0.77	0.72	0.83	0.73	0.80	0.69	0.85	0.75	0.88	0.73
2	0.81	0.80	0.91	0.84	0.96	0.87	0.92	0.82	0.70	0.60	0.76	0.64	0.80	0.65
3	0.86	0.91	0.74	0.81	0.90	0.83	0.94	0.82	0.74	0.76	0.75	0.67	0.79	0.65
4	0.76	0.86	0.91	0.90	0.93	0.89	0.79	0.84	0.81	0.70	0.83	0.67	0.89	0.76
5	0.88	0.91	0.93	0.90	0.91	0.88	0.93	0.86	0.92	0.83	0.90	0.81	0.91	0.79
6	0.91	0.87	0.78	0.74	0.87	0.79	0.75	0.67	0.83	0.78	0.91	0.82	0.83	0.73
7	0.96	0.93	0.95	0.89	0.95	0.88	0.94	0.87	0.95	0.88	0.95	0.87	0.96	0.88
8	0.95	0.86	0.98	0.92	0.98	0.91	0.97	0.90	0.93	0.91	0.94	0.92	0.94	0.92
9	0.84	0.78	0.82	0.71	0.81	0.70	0.86	0.73	0.87	0.79	0.84	0.76	0.89	0.79
10	0.86	0.80	0.74	0.66	0.80	0.74	0.76	0.68	0.84	0.77	0.88	0.85	0.91	0.86

Table 2. Cont.

ID	fSEsEMG _{para%max} fSE sMMG _{para %max}		fSEsEMG _{para%max} Mean P _{di}		fSEsEMG _{para%max} Mean P _{oes}		fSEsEMG _{para%max} Mean P _{mo}		fSE sMMG _{para %max} Mean P _{di}		fSE sMMG _{para %max} Mean P _{oes}		fSE sMMG _{para %max} Mean P _{mo}	
	Lin.	Exp.	Lin.	Exp.	Lin.	Exp.	Lin.	Exp.	Lin.	Exp.	Lin.	Exp.	Lin.	Exp.
11	0.70	0.74	0.83	0.83	0.73	0.73	0.56	0.57	0.91	0.81	0.95	0.87	0.91	0.87
12	0.73	0.76	0.76	0.81	0.83	0.84	0.82	0.81	0.81	0.71	0.87	0.75	0.88	0.74
	0.85	0.83	0.83	0.82	0.88	0.84	0.84	0.81	0.83	0.77	0.88	0.78	0.89	0.77
Median (IQR)	(0.75– 0.90)	(0.77– 0.89)	(0.77– 0.92)	(0.76– 0.90)	(0.80– 0.94)	(0.74– 0.88)	(0.77– 0.93)	(0.71– 0.85)	(0.80– 0.91)	(0.71– 0.82)	(0.84– 0.93)	(0.71– 0.86)	(0.85– 0.91)	(0.73– 0.87)

IQR = interquartile range, Lin. = linear regression model, Exp. = exponential regression model, P_{di} = transdiaphragmatic pressure, P_{oes} = esophageal pressure, P_{mo} = mouth pressure, fSEsEMG_{para%max} = fixed sample entropy measurements of surface electromyography of the parasternal intercostal muscles, fSE | sMMG_{para | %max} = fixed sample entropy measurements of surface mechanomyography of the parasternal intercostal muscles.

Secondly, the relationships between mean P_{di} , mean P_{oes} , and mean P_{mo} and $fSEsEMG_{para\%max}$ measurements shown in Figure 5a were analyzed. Individual analyses showed very strong positive correlations between mean P_{di} , mean P_{oes} , and mean P_{mo} and $fSEsEMG_{para\%max}$ (Table 1). Moreover, the linear and exponential regression results shown in Table 2 indicated that these relationships are better described by linear models than by exponential models. The group $NMC_{P_{di}-EMG_{para}}$ and $NMC_{P_{oes}-EMG_{para}}$ increased very little, not significantly, from load L1 to load L5 (Figure 5b). The group $NMC_{P_{mo}-EMG_{para}}$ increased significantly from load L1 to load L2, but not significantly from load L3 to load L5, thus tending to stabilize around a constant value as the load increases. These results are consistent with the fact that the relationships between mean P_{di} , mean P_{oes} , and mean P_{mo} and $fSEsEMG_{para\%max}$ are better explained by linear than by exponential models.

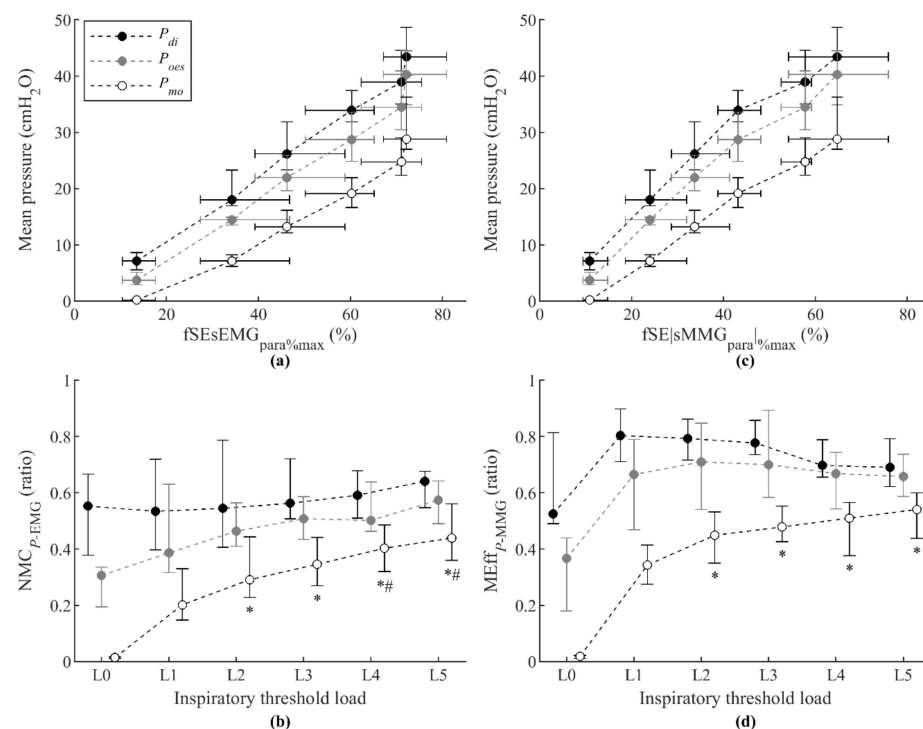


Figure 5. Relationship between respiratory pressures and fixed sample entropy measurements of both surface electromyography ($fSEsEMG_{para\%max}$) (a) and surface mechanomyography ($fSE | sMMG_{para\%max}$) (c) of the parasternal intercostal muscles, and the corresponding neuromechanical coupling ($NMC_{P-EMG_{para}}$) (b) and mechanical efficiency ($MEff_{P-MMG_{para}}$) (d) ratios, during the incremental inspiratory threshold loading protocol. Data points represent median and interquartile range of the 12 subjects for each load. Symbols * and # indicate statistically significant differences with respect to inspiratory threshold loads L1 and L2, respectively.

Finally, the relationships between mean P_{di} , mean P_{oes} , and mean P_{mo} and $fSE | sMMG_{para\%max}$ measurements shown in Figure 5c were analyzed. Individual analyses showed very strong positive correlations between mean P_{di} , mean P_{oes} , and mean P_{mo} and $fSE | sMMG_{para\%max}$ (Table 1). The linear and exponential regression results indicated that these relationships are better described by linear models than by exponential models (Table 2). Accordingly, the group $MEff_{P_{di}-MMG_{para}}$ and $MEff_{P_{oes}-MMG_{para}}$ changed very little, not significantly, from load L1 to load L5 (Figure 5d), and the group $MEff_{P_{mo}-MMG_{para}}$ increased significantly from load L1 to load L2, but not significantly from load L2 to load L5, thus tending to change little as the load increases.

4. Discussion

This study describes for the first time the use of $sMMG_{para}$ as a measure of the mechanical activity of parasternal intercostal muscles, allowing calculation of noninvasive

indices of NMC of parasternal intercostal muscles ($NMC_{MMG-EMG_{para}}$, i.e., the ratio of $fSE | sMMG_{para} | \%_{max}$ to $fSEsEMG_{para}\%_{max}$). $NMC_{MMG-EMG_{para}}$ showed little and not significant changes with progressive increases in inspiratory load between 12% and 60% of PI_{max} . This is due to the mostly linear increase in $fSE | sMMG_{para} | \%_{max}$ relative to $fSEsEMG_{para}\%_{max}$ during threshold loading.

The aforementioned results are equivalent to those found in our previous study using $sMMG_{lic}$ and $sEMG_{lic}$ recordings from the lower chest wall inspiratory muscles [19]. In that study, we showed that both $sEMG_{lic}$ and $sMMG_{lic}$ measurements reflect, in part, the activation of the diaphragm, but also extra-diaphragmatic lower chest wall and abdominal muscle activation [22,33,34], which progressively increases with increasing threshold load to optimize the functioning of the diaphragm [35]. The contribution of the activation of extra-diaphragmatic muscles to $sMMG_{lic}$ and $sEMG_{lic}$ in a similar way was the reason for the parallel increase of $fSE | sMMG_{lic} | \%_{max}$ and $fSEsEMG_{lic}\%_{max}$ during incremental threshold loading, and therefore for the nonsignificant changes in lower chest wall inspiratory muscle NMC from load L1 to load L5.

In the present study, both $fSE | sMMG_{para} | \%_{max}$ and $fSEsEMG_{para}\%_{max}$ measurements have also been found to increase progressively and mostly in parallel with increasing threshold load. The increasing pattern of parasternal intercostal muscle activation during inspiratory threshold loading was previously reported by Reilly et al. [10] using $sEMG_{para}$ measurements in healthy subjects. They reported that, although root-mean-square-based measurements of $oesEMG_{di}\%_{max}$ were consistently greater than those of $sEMG_{para}\%_{max}$, there was a strong relationship between them and they increased mostly linearly during threshold loading. Such coupling between parasternal intercostal muscles and the diaphragm had previously been suggested by De Troyer and Sampson [9], who indicated that parasternal intercostals are involuntarily activated, together with the diaphragm, during inspiratory breathing efforts. Accordingly, $sEMG_{para}$ has been proposed as an alternative noninvasive measure of neural respiratory drive [10,12,14,36].

In non-respiratory skeletal muscles, the relationship between measurements of $sMMG$ and $sEMG$ has been used to characterize some neuromuscular diseases. Orizio et al. [37] analyzed the ratio of $sMMG$ to $sEMG$, which they called electromechanical coupling efficiency, of finger flexors in patients with myotonic dystrophy, who presented lower values as compared to those of control subjects. Barry et al. [38] used the ratio of $sMMG$ to $sEMG$, recorded from the biceps brachii, to study several pediatric muscle diseases. They found a significant reduction in the ratio in affected subjects. The same ratio was used in patients with spastic cerebral palsy by Akataki et al. [39], who found significantly lower ratios of $sMMG$ to $sEMG$ in the patients than in the normal group.

The $sMMG$ signal provides information about muscle contractile properties, reflects the mechanical properties of motor unit activity, and serves as an estimate of muscle force generation [16]. Therefore, relationships between $sMMG$ and $sEMG$ measurements, as expressed by $NMC_{MMG-EMG_{para}}$ in this study, provide muscle-specific noninvasive indices of NMC, which depend mainly on muscle mechanics. In the respiratory system, however, such indices reflect only the first step in the transformation of neural respiratory drive into ventilation. Next steps include the translation of respiratory muscle force into pressure, and the translation of pressure into ventilation. These steps depend on several aspects, such as chest wall geometry, airways resistance, or lung compliance, which can be altered in patients with disordered ventilatory mechanics, such as in COPD or in restrictive lung disease, thus causing neuromechanical and neuroventilatory uncoupling [40]. Therefore, it is desirable to have noninvasive indices of NMC, other than $NMC_{MMG-EMG_{para}}$, capable of reflecting the uncoupling that may occur in the different steps of the transformation of neural respiratory drive into ventilation. Different combinations of measurements of the electrical activation of respiratory muscles, respiratory pressures, and lung volumes have been proposed in previous studies as indices of NMC and neuroventilatory coupling [2,6,19,41–43]. However, the indices proposed in those previous studies involved at least one invasive measurement (i.e., P_{oes} , P_{di} , or $oesEMG_{di}$).

This is the first study to explore the relationships between measurements of $sEMG_{para}$ and $sMMG_{para}$, and measurements of P_{di} , P_{oes} , and P_{mo} to propose noninvasive indices of NMC and MEff of parasternal intercostal muscles. We found progressive and mostly linear increases in $fSEsEMG_{para\%max}$ relative to mean P_{di} , mean P_{oes} , and mean P_{mo} during threshold loading. Analogous results were found between $fSEsEMG_{lic\%max}$ and P_{di} , expressed as a percentage of maximum, in our previous study [19]. Respiratory pressures are considered measurements of global respiratory mechanical output [1], thus reflecting the action of several inspiratory muscles. The linear relationships found between $fSEsEMG_{para\%max}$ and the three different mean pressures (mean P_{di} , mean P_{oes} , and mean P_{mo}) may result therefore from the contribution of progressive activation of parasternal intercostal muscles to $sEMG_{para}$, and of parasternal and other extra-diaphragmatic inspiratory muscles to respiratory pressure measurements. Accordingly, $NMC_{P_{di}-EMG_{para}}$, $NMC_{P_{oes}-EMG_{para}}$, and $NMC_{P_{mo}-EMG_{para}}$ remained almost constant or increased slightly during threshold loading. It is noteworthy, however, that $NMC_{P_{mo}-EMG_{para}}$ increased significantly at the onset of inspiratory loading and from load L1 to load L2, which was due to the low values of P_{mo} during quiet resting breathing. Nevertheless, $NMC_{P_{mo}-EMG_{para}}$ behaved similarly to $NMC_{P_{oes}-EMG_{para}}$ and $NMC_{P_{di}-EMG_{para}}$ as load increased. Progressive and mostly linear increases were also found in $fSE | sMMG_{para} | \%max$ relative to mean P_{di} , mean P_{oes} , and mean P_{mo} during threshold loading. These results are in accordance with those previously found between mean $fSE | sMMG_{lic} |$ and mean P_{di} in our previous study [33]. Accordingly, $MEff_{P_{di}-MMG_{para}}$ and $MEff_{P_{oes}-MMG_{para}}$ showed nonsignificant changes during threshold loading. $MEff_{P_{mo}-MMG_{para}}$, as $NMC_{P_{mo}-EMG_{para}}$, increased significantly at the onset of inspiratory loading and from load L1 to load L2, but behaved similarly to $MEff_{P_{oes}-MMG_{para}}$ and $MEff_{P_{di}-MMG_{para}}$ at higher loads. The $NMC_{P_{mo}-EMG_{para}}$ and $MEff_{P_{mo}-MMG_{para}}$ indices proposed in this study therefore provide noninvasive measurements of the contribution of parasternal intercostal muscle activation to the generation of respiratory pressures.

Parasternal intercostal recordings have the advantage, over lower chest wall inspiratory muscle recordings, of being less affected by the limitations generally associated with surface recordings, such as the difficulty in finding the optimal sensor position or the strong influence of chest wall thickness and subcutaneous fat [44,45]. Moreover, parasternal intercostal recordings are less susceptible to crosstalk from postural chest wall and abdominal muscle activity [21,22]. The noninvasive indices of $NMC_{MMG-EMG_{para}}$, $NMC_{P_{mo}-EMG_{para}}$, and $MEff_{P_{mo}-MMG_{para}}$ proposed in this study would therefore make the evaluation of respiratory muscle function easier and faster to perform, and thus more acceptable in patients with altered respiratory mechanics, such as in obstructive lung disease and neuromuscular disease. Neuroventilatory uncoupling resulting from respiratory muscle weakness and an increased elastic load of the lungs has been related to the degree of dyspnea in patients with neuromuscular disease [6]. Also, in chronic pulmonary diseases, neuromechanical uncoupling has been associated with the perception of breathlessness and limited exercise tolerance [3,5]. The proposed indices would therefore be of potential value to the clinical assessment of these patients.

This study may provide a basis for future research. The clinical utility of the proposed noninvasive NMC and MEff indices requires testing in disease states, since our study dataset was recorded from twelve healthy subjects. The size of the dataset reflects the difficulty in recruiting subjects for studies using invasive measures of diaphragmatic function. The study participants had body mass index values within the normal range. However, it is well known that $sEMG$ and $sMMG$ are affected by the thickness of subcutaneous fat [46,47]. The effect of body mass index on $sMMG_{para}$ and $sEMG_{para}$ measurements should therefore be a focus of future investigation.

5. Conclusions

We have proposed the combined use of P_{mo} and parasternal intercostal $sEMG$ and $sMMG$ recordings to obtain noninvasive indices of NMC and MEff of parasternal intercostal muscles, in healthy adults during an incremental inspiratory threshold loading

protocol. The combination of sMMG_{para} and sEMG_{para} measurements (NMC_{MMG-EMGpara}) provides a muscle-specific noninvasive index of NMC of parasternal intercostal muscles, whose pattern during threshold loading is similar to that previously found in lower chest wall inspiratory muscle NMC. Global noninvasive indices of NMC and MEff of parasternal intercostal muscles have also been proposed by combining P_{mo} measurements and both sEMG_{para} and sMMG_{para} measurements (NMC_{Pmo-EMGpara} and MEff_{Pmo-MMGpara}, respectively), reflecting the contribution of parasternal intercostal muscles to global respiratory mechanical output. Similar patterns have been found in NMC_{Pmo-EMGpara} and MEff_{Pmo-MMGpara}, and their analogous invasive indices, calculated using P_{oes} and P_{di}.

The proposed noninvasive indices derived from P_{mo}, sMMG_{para}, and sEMG_{para} may prove to be useful indices of NMC and MEff of parasternal intercostal muscles, particularly for the assessment of respiratory muscle function using wearable devices. Advances in sensor technologies have led to an increasing trend and interest in the use of wearable and wireless physiological monitoring devices in medicine [48–50]. These devices may contribute to improving the assessment of patients with chronic respiratory diseases by allowing home monitoring of respiratory muscle function in a wireless and noninvasive manner. In this regard, the proposed noninvasive indices of NMC could be easily implemented in a portable device capable of acquiring sEMG and sMMG signals, allowing regular monitoring of patients with impaired respiratory mechanics.

Author Contributions: Conceptualization, M.L.-G., J.M., C.J.J. and R.J.; methodology, M.L.-G., L.E.-P., A.T., G.F.R., C.J.J. and R.J.; software, M.L.-G.; validation, M.L.-G., L.E.-P., A.T., G.F.R., C.J.J. and R.J.; formal analysis, M.L.-G.; investigation, M.L.-G., L.E.-P., A.T., G.F.R., C.J.J. and R.J.; writing—original draft preparation, M.L.-G.; writing—review and editing, M.L.-G., L.E.-P., A.T., G.F.R., C.J.J. and R.J.; visualization, M.L.-G.; supervision, J.M., C.J.J. and R.J. All authors have read and agreed to the published version of the manuscript.

Funding: This work was supported in part by the Generalitat de Catalunya (CERCA Programme and GRC 2017 SGR 01770), the Gobierno de España (RTI2018-098472-B-I00 MCIU/AEI/FEDER, UE), and the Biomedical Research Networking Centre in Bioengineering, Biomaterials and Nanomedicine (CIBER-BBN, Instituto de Salud Carlos III/FEDER). Manuel Lozano-García and Luis Estrada-Petrocelli were the recipients of two European Respiratory Society Fellowships (ERS LTRF 2015-5185 and ERS LTRF 2017 01-00086, respectively).

Institutional Review Board Statement: The study was conducted according to the guidelines of the Declaration of Helsinki, and approved by the National Health Service Health Research Authority (National Research Ethics Service Committee London—Dulwich 05/Q0703).

Informed Consent Statement: Written informed consent was obtained from all subjects involved in the study.

Data Availability Statement: The data presented in this study are available from the corresponding author on reasonable request.

Conflicts of Interest: The authors declare no conflict of interest. The funders had no role in the design of the study; in the collection, analyses, or interpretation of data; in the writing of the manuscript, or in the decision to publish the results.

References

1. Laveneziana, P.; Albuquerque, A.; Aliverti, A.; Babb, T.; Barreiro, E.; Dres, M.; Dubé, B.P.; Fauroux, B.; Gea, J.; Guenette, J.A.; et al. ERS statement on respiratory muscle testing at rest and during exercise. *Eur. Respir. J.* **2019**, *53*, 1801214. [[CrossRef](#)] [[PubMed](#)]
2. Gorini, M.; Spinelli, A.; Ginanni, R.; Duranti, R.; Gigliotti, F.; Scano, G. Neural Respiratory Drive and Neuromuscular Coupling in Patients with Chronic Obstructive Pulmonary Disease (COPD). *Chest* **1990**, *98*, 1179–1186. [[CrossRef](#)] [[PubMed](#)]
3. Duiverman, M.L.; de Boer, E.W.J.; van Eykern, L.A.; de Greef, M.H.G.; Jansen, D.F.; Wempe, J.B.; Kerstjens, H.A.M.; Wijkstra, P.J. Respiratory muscle activity and dyspnea during exercise in chronic obstructive pulmonary disease. *Respir. Physiol. Neurobiol.* **2009**, *167*, 195–200. [[CrossRef](#)] [[PubMed](#)]
4. Druz, W.S.; Sharp, J.T. Electrical and mechanical activity of the diaphragm accompanying body position in severe chronic obstructive pulmonary disease. *Am. Rev. Respir. Dis.* **1982**, *125*, 275–280. [[PubMed](#)]

5. O'Donnell, D.E.; Ora, J.; Webb, K.A.; Laveneziana, P.; Jensen, D. Mechanisms of activity-related dyspnea in pulmonary diseases. *Respir. Physiol. Neurobiol.* **2009**, *167*, 116–132.
6. Lanini, B.; Misuri, G.; Gigliotti, F.; Iandelli, I.; Pizzi, A.; Romagnoli, I.; Scano, G. Perception of dyspnea in patients with neuromuscular disease. *Chest* **2001**, *120*, 402–408. [[CrossRef](#)]
7. Mead, J.; Loring, S.H. Analysis of volume displacement and length changes of the diaphragm during breathing. *J. Appl. Physiol.* **1982**, *53*, 750–755. [[CrossRef](#)] [[PubMed](#)]
8. Luo, Y.M.; Moxham, J.; Polkey, M.I. Diaphragm electromyography using an oesophageal catheter: Current concepts. *Clin. Sci.* **2008**, *115*, 233–244. [[CrossRef](#)] [[PubMed](#)]
9. De Troyer, A.; Sampson, M.G. Activation of the parasternal intercostals during breathing efforts in human subjects. *J. Appl. Physiol. Respir. Environ. Exerc. Physiol.* **1982**, *52*, 524–529. [[CrossRef](#)]
10. Reilly, C.C.; Jolley, C.J.; Ward, K.; MacBean, V.; Moxham, J.; Rafferty, G.F. Neural respiratory drive measured during inspiratory threshold loading and acute hypercapnia in healthy individuals. *Exp. Physiol.* **2013**, *98*, 1190–1198. [[CrossRef](#)]
11. Lin, L.; Guan, L.; Wu, W.; Chen, R. Correlation of surface respiratory electromyography with esophageal diaphragm electromyography. *Respir. Physiol. Neurobiol.* **2019**, *259*, 45–52. [[CrossRef](#)]
12. Reilly, C.C.; Ward, K.; Jolley, C.J.; Lunt, A.C.; Steier, J.; Elston, C.; Polkey, M.I.; Rafferty, G.F.; Moxham, J. Neural respiratory drive, pulmonary mechanics and breathlessness in patients with cystic fibrosis. *Thorax* **2011**, *66*, 240–246. [[CrossRef](#)] [[PubMed](#)]
13. Schmidt, M.; Kindler, F.; Gottfried, S.B.; Raux, M.; Hug, F.; Similowski, T.; Demoule, A. Dyspnea and surface inspiratory electromyograms in mechanically ventilated patients. *Intensive Care Med.* **2013**, *39*, 1368–1376. [[CrossRef](#)] [[PubMed](#)]
14. Murphy, P.B.; Kumar, A.; Reilly, C.; Jolley, C.; Walterspercher, S.; Fedele, F.; Hopkinson, N.S.; Man, W.D.-C.; Polkey, M.I.; Moxham, J.; et al. Neural respiratory drive as a physiological biomarker to monitor change during acute exacerbations of COPD. *Thorax* **2011**, *66*, 602–608. [[CrossRef](#)]
15. Suh, E.-S.; Mandal, S.; Harding, R.; Ramsay, M.; Kamalanathan, M.; Henderson, K.; O'Kane, K.; Douiri, A.; Hopkinson, N.S.; Polkey, M.I.; et al. Neural respiratory drive predicts clinical deterioration and safe discharge in exacerbations of COPD. *Thorax* **2015**, *70*, 1123–1130. [[CrossRef](#)] [[PubMed](#)]
16. Orizio, C.; Gobbo, M. Mechanomyography. In *Wiley Encyclopedia of Biomedical Engineering*; John Wiley & Sons, Inc.: Hoboken, NJ, USA, 2006.
17. Madeleine, P.; Bajaj, P.; Søgaard, K.; Arendt-Nielsen, L. Mechanomyography and electromyography force relationships during concentric, isometric and eccentric contractions. *J. Electromyogr. Kinesiol.* **2001**, *11*, 113–121. [[CrossRef](#)]
18. Ebersole, K.T.; Malek, D.M. Fatigue and the electromechanical efficiency of the vastus medialis and vastus lateralis muscles. *J. Athl. Train.* **2008**, *43*, 152–156. [[CrossRef](#)] [[PubMed](#)]
19. Lozano-Garcia, M.; Estrada-Petrocelli, L.; Moxham, J.; Rafferty, G.F.; Torres, A.; Jolley, C.J.; Jane, R. Noninvasive Assessment of Inspiratory Muscle Neuromechanical Coupling During Inspiratory Threshold Loading. *IEEE Access* **2019**, *7*, 183634–183646. [[CrossRef](#)]
20. Sarlabous, L.; Torres, A.; Fiz, J.A.; Gea, J.; Martínez-Llorens, J.M.; Jané, R. Efficiency of mechanical activation of inspiratory muscles in COPD using sample entropy. *Eur. Respir. J.* **2015**, *46*, 1808–1811. [[CrossRef](#)]
21. De Troyer, A.; Estenne, M.; Ninane, V.; Van Gansbeke, D.; Gorini, M. Transversus abdominis muscle function in humans. *J. Appl. Physiol.* **1990**, *68*, 1010–1016. [[CrossRef](#)]
22. Sinderby, C.; Friberg, S.; Comtois, N.; Grassino, A. Chest wall muscle cross talk in canine costal diaphragm electromyogram. *J. Appl. Physiol.* **1996**, *81*, 2312–2327. [[CrossRef](#)] [[PubMed](#)]
23. Finucane, K.E.; Panizza, J.A.; Singh, B. Efficiency of the normal human diaphragm with hyperinflation. *J. Appl. Physiol.* **2005**, *99*, 1402–1411. [[CrossRef](#)] [[PubMed](#)]
24. Finucane, K.E.; Singh, B. Human diaphragm efficiency estimated as power output relative to activation increases with hypercapnic hyperpnea. *J. Appl. Physiol.* **2009**, *107*, 1397–1405. [[CrossRef](#)] [[PubMed](#)]
25. Finucane, K.E.; Singh, B. Diaphragm efficiency estimated as power output relative to activation in chronic obstructive pulmonary disease. *J. Appl. Physiol.* **2012**, *113*, 1567–1575. [[CrossRef](#)] [[PubMed](#)]
26. Laghi, F.; Shaikh, H.S.; Morales, D.; Sinderby, C.; Jubran, A.; Tobin, M.J. Diaphragmatic neuromechanical coupling and mechanisms of hypercapnia during inspiratory loading. *Respir. Physiol. Neurobiol.* **2014**, *198*, 32–41. [[CrossRef](#)] [[PubMed](#)]
27. MacBean, V.; Hughes, C.; Nicol, G.; Reilly, C.C.; Rafferty, G.F. Measurement of neural respiratory drive via parasternal intercostal electromyography in healthy adult subjects. *Physiol. Meas.* **2016**, *37*, 2050–2063. [[CrossRef](#)] [[PubMed](#)]
28. Jolley, C.J.; Luo, Y.M.; Steier, J.; Reilly, C.; Seymour, J.; Lunt, A.; Ward, K.; Rafferty, G.F.; Polkey, M.I.; Moxham, J. Neural respiratory drive in healthy subjects and in COPD. *Eur. Respir. J.* **2009**, *33*, 289–297. [[CrossRef](#)] [[PubMed](#)]
29. Ibitoye, M.O.; Hamzaid, N.A.; Zuniga, J.M.; Hasnan, N.; Wahab, A.K.A. Mechanomyographic parameter extraction methods: An appraisal for clinical applications. *Sensors* **2014**, *14*, 22940–22970. [[CrossRef](#)] [[PubMed](#)]
30. Sarlabous, L.; Torres, A.; Fiz, J.A.; Jané, R. Evidence towards improved estimation of respiratory muscle effort from diaphragm mechanomyographic signals with cardiac vibration interference using sample entropy with fixed tolerance values. *PLoS ONE* **2014**, *9*, e88902. [[CrossRef](#)]
31. Estrada, L.; Torres, A.; Sarlabous, L.; Jané, R. Improvement in neural respiratory drive estimation from diaphragm electromyographic signals using fixed sample entropy. *IEEE J. Biomed. Heal. Informatics* **2016**, *20*, 476–485. [[CrossRef](#)]

32. Lozano-García, M.; Estrada, L.; Jané, R. Performance evaluation of fixed sample entropy in myographic signals for inspiratory muscle activity estimation. *Entropy* **2019**, *21*, 183.
33. Lozano-García, M.; Sarlabous, L.; Moxham, J.; Rafferty, G.F.; Torres, A.; Jané, R.; Jolley, C.J. Surface mechanomyography and electromyography provide non-invasive indices of inspiratory muscle force and activation in healthy subjects. *Sci. Rep.* **2018**, *8*, 16921.
34. Demoule, A.; Verin, E.; Locher, C.; Derenne, J.P.; Similowski, T. Validation of surface recordings of the diaphragm response to transcranial magnetic stimulation in humans. *J. Appl. Physiol.* **2003**, *94*, 453–461. [[CrossRef](#)] [[PubMed](#)]
35. Goldman, M.D.; Grassino, A.; Mead, J.; Sears, T.A. Mechanics of the human diaphragm during voluntary contraction: Dynamics. *J. Appl. Physiol.* **1978**, *44*, 840–848. [[CrossRef](#)] [[PubMed](#)]
36. Reilly, C.C.; Jolley, C.J.; Elston, C.; Moxham, J.; Rafferty, G.F. Measurement of parasternal intercostal electromyogram during an infective exacerbation in patients with cystic fibrosis. *Eur. Respir. J.* **2012**, *40*, 977–981. [[CrossRef](#)]
37. Orizio, C.; Esposito, F.; Sansone, V.; Parrinello, G.; Meola, G.; Veicsteinas, A. Muscle surface mechanical and electrical activities in myotonic dystrophy. *Electromyogr. Clin. Neurophysiol.* **1997**, *37*, 231–239. [[PubMed](#)]
38. Barry, D.T.; Gordon, K.E.; Hinton, G.G. Acoustic and surface EMG diagnosis of pediatric muscle disease. *Muscle Nerve* **1990**, *13*, 286–290. [[CrossRef](#)] [[PubMed](#)]
39. Akasaki, K.; Mita, K.; Itoh, K.; Suzuki, N.; Watakabe, M. Acoustic and electrical activities during voluntary isometric contraction of biceps brachii muscles in patients with spastic cerebral palsy. *Muscle Nerve* **1996**, *19*, 1252–1257. [[CrossRef](#)]
40. Jensen, D.; Pattinson, K.; Jolley, C.J. Mechanisms of Breathlessness. In *European Respiratory Society Monograph*; Bausewein, C., Currow, D., Johnson, M., Eds.; European Respiratory Society Journals: Lausanne, Switzerland, 2016; pp. 111–113.
41. Laghi, F.; Jubran, A.; Topeli, A.; Fahey, P.J.; Garrity, E.R.; Arcidi, J.M.; de Pinto, D.J.; Edwards, L.C.; Tobin, M.J. Effect of Lung Volume Reduction Surgery on Neuromechanical Coupling of the Diaphragm. *Am. J. Respir. Crit. Care Med.* **1998**, *157*, 475–483. [[CrossRef](#)]
42. O'Donnell, D.E.; Bertley, J.C.; Chau, L.K.; Webb, K.A. Qualitative aspects of exertional breathlessness in chronic airflow limitation: Pathophysiologic mechanisms. *Am. J. Respir. Crit. Care Med.* **1997**, *155*, 109–115.
43. Jolley, C.J.; Luo, Y.M.; Steier, J.; Rafferty, G.F.; Polkey, M.I.; Moxham, J. Neural respiratory drive and breathlessness in COPD. *Eur. Respir. J.* **2015**, *45*, 355–364. [[CrossRef](#)] [[PubMed](#)]
44. Glerant, J.C.; Mustafa, N.; Man, W.D.; Luo, Y.M.; Rafferty, G.; Polkey, M.I.; Moxham, J. Diaphragm electromyograms recorded from multiple surface electrodes following magnetic stimulation. *Eur. Respir. J.* **2006**, *27*, 334–342. [[CrossRef](#)]
45. Dos Reis, I.M.M.; Ohara, D.G.; Januário, L.B.; Basso-Vanelli, R.P.; Oliveira, A.B.; Jamami, M. Surface electromyography in inspiratory muscles in adults and elderly individuals: A systematic review. *J. Electromyogr. Kinesiol.* **2019**, *44*, 139–155. [[CrossRef](#)] [[PubMed](#)]
46. Scheeren, E.M.; Mineiro, L.; Neves, E.B.; Krueger, E.; Nogueira Neto, G.N.; Nohama, P.; Scheeren, E.M.; Mineiro, L.; Neves, E.B.; Krueger, E.; et al. Influence of subcutaneous fat on mechanomyographic signals at three levels of voluntary effort. *Res. Biomed. Eng.* **2017**, *32*, 307–317. [[CrossRef](#)]
47. Nordander, C.; Willner, J.; Hansson, G.-A.; Larsson, B.; Unge, J.; Granquist, L.; Skerfving, S. Influence of the subcutaneous fat layer, as measured by ultrasound, skinfold calipers and BMI, on the EMG amplitude. *Eur. J. Appl. Physiol.* **2003**, *89*, 514–519. [[CrossRef](#)] [[PubMed](#)]
48. Ràfols-De-Urquía, M.; Estrada, L.; Estévez-Piorno, J.; Sarlabous, L.; Jané, R.; Torres, A. Evaluation of a Wearable Device to Determine Cardiorespiratory Parameters from Surface Diaphragm Electromyography. *IEEE J. Biomed. Heal. Informatics* **2019**, *23*, 1964–1971.
49. Xu, J.; Konijnenburg, M.; Ha, H.; Van Wegberg, R.; Song, S.; Blanco-Almazán, D.; Van Hoof, C.; Van Helleputte, N. A 36 μ W 1.1 mm² Reconfigurable Analog Front-End for Cardiovascular and Respiratory Signals Recording. *IEEE Trans. Biomed. Circuits Syst.* **2018**, *12*, 774–783. [[CrossRef](#)]
50. Song, S.; Konijnenburg, M.; Van Wegberg, R.; Xu, J.; Ha, H.; Sijbers, W.; Stanzione, S.; Biswas, D.; Breeschoten, A.; Vis, P.; et al. A 769 μ W Battery-Powered Single-Chip SoC with BLE for Multi-modal Vital Sign Monitoring Health Patches. *IEEE Trans. Biomed. Circuits Syst.* **2019**, *13*, 1506–1517. [[CrossRef](#)]